Enabling Forbidden Dark Matter

James Cline,[1,2,*] Hongwan Liu,[3,†] Tracy Slatyer,[3,‡] and Wei Xue[3,§]

[1] *CERN, Theoretical Physics Department, Geneva, Switzerland*
[2] *Department of Physics, McGill University, 3600 Rue University, Montreal, Quebec, Canada H3A 2T8*
[3] *Center for Theoretical Physics, Massachusetts Institute of Technology, Cambridge, MA 02139, U.S.A.*

The thermal relic density of dark matter is conventionally set by two-body annihilations. We point out that in many simple models, $3 \to 2$ annihilations can play an important role in determining the relic density over a broad range of model parameters. This occurs when the two-body annihilation is kinematically forbidden, but the $3 \to 2$ process is allowed; we call this scenario *Not-Forbidden Dark Matter*. We illustrate this mechanism for a vector portal dark matter model, showing that for a dark matter mass of $m_\chi \sim$ MeV - 10 GeV, $3 \to 2$ processes not only lead to the observed relic density, but also imply a self-interaction cross section that can solve the cusp/core problem. This can be accomplished while remaining consistent with stringent CMB constraints on light dark matter, and can potentially be discovered at future direct detection experiments.

arXiv:1702.07716v1 [hep-ph] 24 Feb 2017

I. INTRODUCTION

The particle physics nature of dark matter (DM) is still a mystery despite undeniable evidence of its gravitational interactions. The observed relic abundance of DM may provide a clue to its non-gravitational interactions, as in the classic weakly interacting massive particle scenario, where the freezeout of $2 \to 2$ annihilation of DM particles to the standard model (SM) particles sets the late-time abundance of DM. Many variations on the standard thermal freezeout scenario have recently been considered (e.g. [1–25]); in this article, we point out that even for simple and weakly-coupled dark sectors, $3 \to 2$ annihilations – as illustrated in fig. 1 – can play a critical role.

For weakly-coupled DM, $3 \to 2$ processes are usually considered to be subdominant to their $2 \to 2$ counterparts at the time of freezeout, but if the latter are kinematically suppressed while $3 \to 2$ is unsuppressed, the situation is more complex. This can occur when the DM couples to a "mediator" particle with a mass is somewhat larger than that of the DM itself, as might arise in a hidden sector characterized by a single scale.

Kinematic suppression of $2 \to 2$ annihilation, leading to a novel cosmological history during freezeout, was previously invoked in the "Forbidden DM" [9] and "Impeded DM" [25] scenarios; the new feature in our study is the presence of a kinematically allowed dark-sector $3 \to 2$ annihilation channel. We refer to this scenario as *Not-Forbidden Dark Matter* (NFDM). The $3 \to 2$ channel is also important in the Strongly Interacting Massive Particle (SIMP) scenario [3], but work on SIMPs has focused on strongly coupled theories with scalar DM [4], whereas NFDM is a generic mechanism in hidden sector or multicomponent DM models, in which the DM may be fermionic or bosonic, the coupling can be strong or weak, and the suppression of $2 \to 2$ is kinematical.

* jcline@physics.mcgill.ca
† hongwan@mit.edu
‡ tslatyer@mit.edu
§ weixue@mit.edu

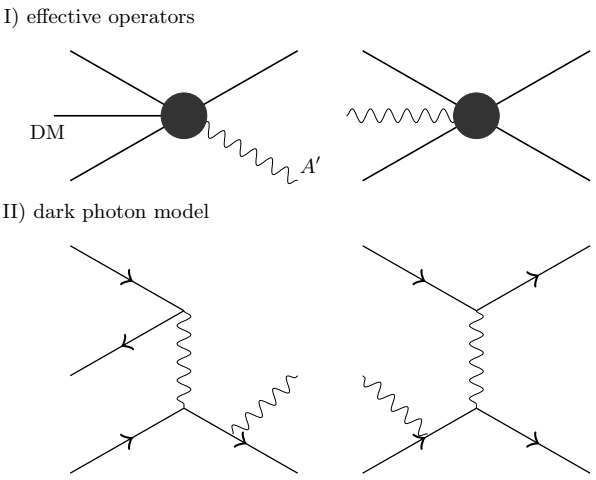

FIG. 1. Schematic description of *Not-Forbidden Dark Matter* (NFDM) paradigm. I) effective operators for the $3 \to 2$ scattering processes; II) ultraviolet completion of the effective theory in the dark photon + dark matter model.

We illustrate our paradigm with one of the simplest DM models, where the DM is a Dirac fermion that is charged under a hidden $U(1)$ symmetry, with dark gauge boson A'. This mediator can provide a portal to the SM by having a small coupling to the electromagnetic current J^μ_{EM} through kinetic mixing,

$$\mathcal{L} = \bar{\chi}(i\not{D} - m_\chi)\chi + \tfrac{1}{2}m^2_{A'}\, A'_\mu A'^\mu + e\epsilon A'_\mu J^\mu_{EM} \ . \quad (1)$$

The gauge coupling is $\alpha' = g'^2/4\pi$. We can consistently assume that the dark Higgs boson giving mass to A' is very heavy and can be neglected in the effective description [26]. Depending upon the size of the kinetic mixing parameter ϵ, there are two possible regimes of interest:

(1) ϵ is relatively large, such that the hidden sector and the SM sector have the same temperature before DM freezeout, while ϵ is still small enough so that $3 \to 2$ and $2 \to 2$ reactions involving only hidden sector particles dominate over annihilation of χ to SM particles;

(2) For sufficiently small $\epsilon \lesssim 10^{-8}$, the hidden sector will have its own temperature and in the limit $\epsilon \to 0$, it becomes secluded: both χ and A' contribute to the ultimate DM density.

In section II, we discuss the freezeout history of the NFDM model, and by solving the Boltzmann equations, we determine the dark sector parameter values $\{m_\chi, m_{A'}, \epsilon\}$ that are consistent with the observed relic density. In section III we incorporate constraints from a variety of astrophysical and laboratory searches, showing that a significant parameter region is allowed while realizing the NFDM mechanism. Conclusions are given in section IV. In the supplemental material, we present a more detailed account of how the order of freezeout of the various reactions determines the relic abundance; the dependence of our results on the temperature of the dark sector; how the constraints change with $m_{A'}/m_\chi$, and cross sections for the relevant scattering processes.

II. COSMOLOGY

Previous studies of the vector-portal DM model, shown in eq. (1), have divided the parameter space into two broad regions: $m_\chi < m_{A'}$ or $m_\chi > m_{A'}$. In the latter case, the dominant process at the epoch of thermal freezeout is $\chi\bar{\chi} \to A'A'$ followed by A' decays to SM particles, whereas when $m_\chi < m_{A'}$, the s-channel annihilation $\chi\bar{\chi} \to f\bar{f}$ to SM particles f via off-shell A' is dominant. This regime is ruled out for $m_\chi \sim$ MeV-GeV by CMB constraints [27–31].

In the present work, however, we are interested in the intermediate region $m_\chi \lesssim m_{A'}$, where it is possible for the $3 \to 2$ scatterings $\chi\chi\bar{\chi} \to \chi A'$ or $\chi\bar{\chi}A' \to \chi\bar{\chi}$ to have an important effect on the dark matter abundance. The system is governed by the coupled Boltzmann equations for the χ and A' densities,

$$\frac{dn_\chi}{dt} + 3Hn_\chi = -\frac{1}{4}\langle\sigma v^2\rangle_{\substack{\chi\chi\bar{\chi}\\ \to\chi A'}}\left(n_\chi^3 - n_{\chi,0}^2 n_\chi \frac{n_{A'}}{n_{A',0}}\right) + \langle\sigma v\rangle_{\substack{A'A'\\ \to\bar{\chi}\chi}}\left(n_{A'}^2 - n_{A',0}^2\frac{n_\chi^2}{n_{\chi,0}^2}\right), \quad (2)$$

$$\frac{dn_{A'}}{dt} + 3Hn_{A'} = \frac{1}{8}\langle\sigma v^2\rangle_{\substack{\chi\chi\bar{\chi}\\ \to\chi A'}}\left(n_\chi^3 - n_{\chi,0}^2 n_\chi \frac{n_{A'}}{n_{A',0}}\right) - \frac{1}{4}\left(\langle\sigma v^2\rangle_{\substack{\chi\bar{\chi}A'\\ \to\chi\bar{\chi}}} + \langle\sigma v^2\rangle_{\substack{\chi\chi A'\\ \to\chi\chi}}\right)\left(n_\chi^2 n_{A'} - n_\chi^2 n_{A',0}\right) - \langle\sigma v\rangle_{\substack{A'A'\\ \to\bar{\chi}\chi}}\left(n_{A'}^2 - n_{A',0}^2\frac{n_\chi^2}{n_{\chi,0}^2}\right) - \Gamma_{A'\to f\bar{f}}\left(n_{A'} - n_{A',0}\right) \quad (3)$$

where $n_\chi\,(n_{\chi,0})$ denotes the (equilibrium) density of $\chi + \bar{\chi}$, and similarly $n'_A\,(n_{A',0})$ for the dark photon. The 1/4 is the symmetry factor for Dirac DM. The reaction $\chi\bar{\chi}A' \to \chi\bar{\chi}$ turns out to be important only in the case of $m_{A'}/m_\chi < 1$ and $\epsilon = 0$ in Sec. II B. Expressions for the cross sections are given in the supplementary material.

We will focus on the two regimes where (1) the hidden sector and the SM remain in thermal equilibrium, requiring values of the kinetic mixing $\epsilon \gtrsim 10^{-7}$ (but still small enough to avoid dominance of the $\chi\bar{\chi} \to e^+e^-$ process); (2) the hidden sector is secluded from the SM, $\epsilon \to 0$.

A. Kinetic equilibrium with the SM

For sufficiently large ϵ, the scattering process $\chi e^\pm \to \chi e^\pm$ is fast enough to keep the dark and visible sectors in kinetic equilibrium, $T_{DM} = T_{SM}$. By comparing the rate inferred from the $\chi e^\pm \to \chi e^\pm$ cross section to the Hubble rate H at DM freezeout, we estimate the condition to be

$$\epsilon \gtrsim 10^{-8}\left(\frac{0.1}{\alpha'}\right)^{1/2}\left(\frac{m_\chi}{1\,\mathrm{GeV}}\right)^{1/2}, \quad (4)$$

taking $x_f \sim 20$, the $e^\pm$ to be relativistic, and $m_{A'} \simeq m_\chi$. This leaves a significant range of $\epsilon \lesssim 10^{-4} - 10^{-6}$, depending upon m_χ, such that A'-mediated annihilations $\chi\bar{\chi} \to e^+e^-$ are out of equilibrium (a requirement of our scenario), as will be shown below.

We take the dark sector masses to be in the ranges $m_\chi \lesssim 10$ GeV and $m_\chi \lesssim m_{A'} < 2m_\chi$. The lower bound on $m_{A'}$ makes $\chi\bar{\chi} \to A'A'$ kinematically inaccessible, while the upper bound forbids the $A' \to \chi\bar{\chi}$ decay channel. If $m_{A'} > 2m_\chi$, the number-changing process $\chi\chi\bar{\chi} \to A'\chi$ effectively becomes number-conserving, $\chi\chi\bar{\chi} \to \chi\chi\bar{\chi}$. In terms of the parameter $r \equiv m_{A'}/m_\chi$, the relevant range is thus $1 \lesssim r \lesssim 2$.

It is enlightening to compare the equilibrium rates (per χ particle) of the $3 \to 2$ and $2 \to 2$ reactions in eq. (2-3), $\Gamma_{\substack{\chi\chi\bar{\chi}\\ \to\chi A'}} \sim \langle\sigma v^2\rangle_{\substack{\chi\chi\bar{\chi}\\ \to\chi A'}} n_{\chi,0}^2$ and $\Gamma_{\substack{A'A'\\ \to\bar{\chi}\chi}} \sim \langle\sigma v\rangle_{\substack{A'A'\\ \to\bar{\chi}\chi}} n_{A',0}^2/n_{\chi,0}$. From the exponential dependences in the equilibrium number densities, $n_{i,0} \sim \exp(-m_i/T)$, we find that if $m_{A'} \gtrsim \frac{3}{2}m_\chi$, the $3 \to 2$ reaction will be exponentially enhanced with respect to the $2 \to 2$ reaction at low temperatures. We will verify below that the physics of DM thermal freezeout changes qualitatively near $m_{A'} \sim 1.5\,m_\chi$, i.e. $r \sim 1.5$.

The Boltzmann equations are solved numerically, and the results shown in fig 2. As an example, the left plot (a) illustrates the evolution of the χ and A' abundances as a function of $x \equiv m_\chi/T$ with $m_\chi = 0.3$ GeV, gauge coupling $\alpha' = 1$, kinetic mixing $\epsilon = 10^{-6}$ and the ratio $r = 1.9$. In the case with only $2 \to 2$ annihilation, the DM abundance would reach its relic value at $x_f \sim 20$; in our NFDM case, in contrast, the $3 \to 2$ processes and decay of the A' control the freezeout, and their interplay leads to an extended freezeout continuing to $x_f \sim 60$. If we neglect the $3 \to 2$ process the resulting abundance is overestimated by several orders of magnitude. It is noteworthy that $Y_{A'}$ departs from the equilibrium abundance at late times, even though the rate for $A' \to e^+e^-$ exceeds

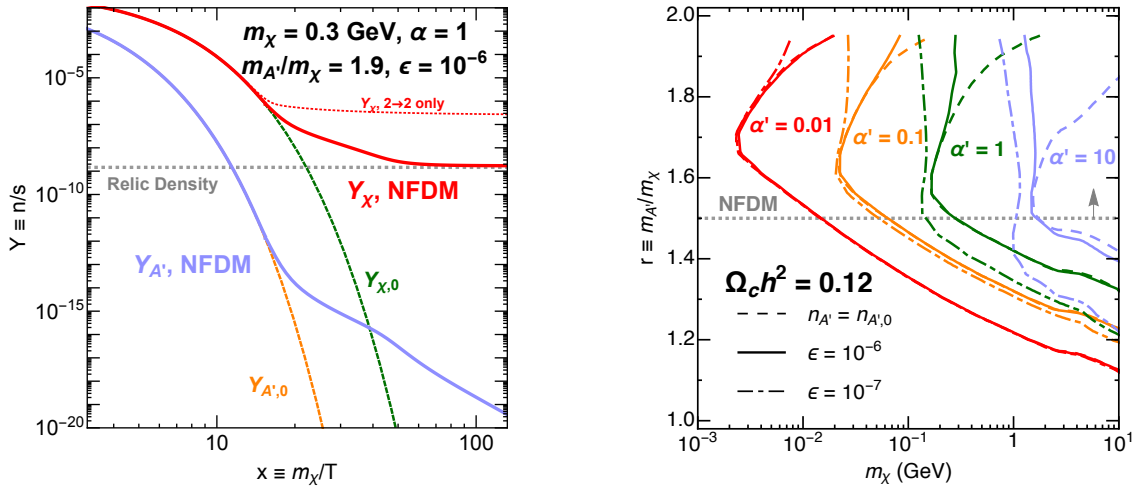

FIG. 2. Relic density in the NFDM scenario, assuming kinetic equilibrium of the dark sector with the SM. (a) The evolution of the energy density of χ (red) and A' (blue) for all processes (bold) and the corresponding energy density of χ excluding the $3 \to 2$ process (red, dotted). The equilibrium distribution of χ (orange) and A' (purple) are also shown for reference; (b) contours of the observed present-day relic density in the m_χ-r plane for different values of the coupling constant α'.

the Hubble rate, because the $3 \to 2$ or $2 \to 2$ processes can also strongly affect the evolution of $n_{A'}$ (in the example of fig 2(a) it is the $3 \to 2$ rate that is relevant), as we will discuss in more detail in the supplemental materials.

In fig. 2(b) we plot the contours in the m_χ-r plane matching the observed relic density [30], for several values of α' and ϵ. $n_{A'} = n_{A',0}$ correponds to large ϵ, where the rate for $A' \to e^+e^-$ dominates the rates for either of the two annihilation processes that generate A's. The region $r \lesssim 1.5$ corresponds to the Forbidden DM regime, and ref. [9] studied this regime with the assumption of $n_{A'} = n_{A',0}$. Our interest is in the NFDM region $1.5 \lesssim r < 2$, where the $3 \to 2$ processes lead to qualitatively different behavior, which can be counterintuitive relative to one's experience with more conventional DM freezeout.

Normally the DM relic density is set by the strongest annihilation channel, which is also the last to freeze out, since only a single Boltzmann equation for DM is considered. This applies when ϵ is large, forcing $n_{A'} \simeq n_{A',0}$ (dashed contours), so that the Boltzmann equation for A' is trivially satisfied. These contours turn to the right as $r \to 2$ because the $3 \to 2$ cross section diverges, $\langle \sigma v^2 \rangle_{\substack{\chi\chi\bar{\chi} \\ \to \chi A'}} \propto \alpha'^3 m_\chi^{-5} (r-2)^{-7/2}$, and $Y_\chi \sim x_f^2 / [m_{pl} m_\chi^2 \langle \sigma v^2 \rangle_{\substack{\chi\chi\bar{\chi} \\ \to \chi A'}}]^{1/2}$. Thus obtaining the correct relic density as $r \to 2$ requires a larger value of m_χ.

In contrast, for moderate values of ϵ, the NFDM mechanism applies, where the two coupled Boltzmann equations must be solved together. In general, we find that typically the *two strongest processes* (either annihilations or decays) keep the coupled system in equilibrium until the rate for one process (per χ particle) becomes comparable to the Hubble rate, and thus any weaker processes are not relevant for determining the relic abundance. In this regime, typically the decay of $A' \to e^+e^-$ and either the $3 \to 2$ or $2 \to 2$ annihilation are the relevant processes. In particular, for $r \gtrsim 1.5 - 1.8$, the $3 \to 2$ scatterings are faster than $2 \to 2$, and so they dominate the freezeout, as shown in fig. 2(a). The combination of $3 \to 2$ scatterings and A' decays can lead to a non-equilibrium density for the A' particles during the freezeout of the $3 \to 2$ process if ϵ is sufficiently small (e.g. $\epsilon \sim 10^{-6} - 10^{-7}$), resulting in a lengthy freezeout and an ϵ-dependent relic density. This behavior corresponds to the divergence of the dashed and solid contours in fig. 2(b) at large r. Further details are given in the supplementary material.

B. Secluded hidden sector

Next we consider the limit of $\epsilon \to 0$, so that the dark photon is effectively stable, and the hidden sector is secluded. This analysis can be easily applied to multi-component DM models. If the dark sector consisted only of mass-gapped particles χ and A', the DM temperature would remain too high [12], leading to warm or hot dark matter. To avoid this, we assume that χ couples additionally to a species of dark radiation ψ, strongly enough to maintain thermal equilibrium in the dark sector so that the DM temperature redshifts with the Hubble expansion in the conventional manner, $T \sim 1/a$. However, the coupling of ψ to χ should be sufficiently weak that annihilation of $\chi\bar{\chi} \to \psi\psi$ is negligible during freezeout, to make the NFDM freezeout mechanism dominate over conventional $2 \to 2$ annihilation.

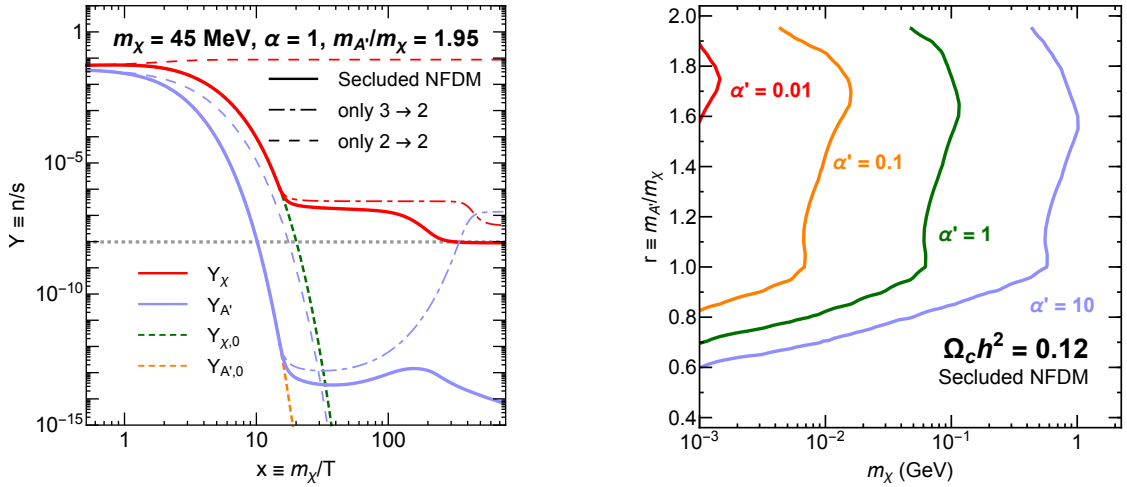

(a) (b)

FIG. 3. NFDM, secluded hidden sector: (a) The evolution of energy density of χ (red) and A' (blue) with (solid) all relevant processes; (dotted) only $3 \to 2$ processes; (dashed) only $2 \to 2$ processes. The equilibrium distribution of χ (orange) and A' (purple) are also shown for reference; (b) contours of the observed present-day relic density in the m_χ-r parameter space for different coupling constants α'.

The dark sector has its own temperature T_d which need not be the same as that of the visible sector, $T_{\rm SM}$; it is determined by details of the thermal cosmological history such as efficiency of reheating into the dark sector after inflation. The relic abundance in this case depends upon the unknown parameter $\gamma \equiv T_d/T_{\rm SM}$, but (as we will show), in a simple way: $Y_\chi \propto \gamma^{p(r)}$ where $p(r) \sim 1.6-1.8$ depends upon the mass ratio $r = m_{A'}/m_\chi$. Here we illustrate the case of $\gamma = 1$.

The evolution of n_χ and $n_{A'}$ for the secluded dark sector is shown in fig. 3(a), taking $m_\chi = 45\,\text{MeV}$, $\alpha' = 1$, $r = 1.95$ as an example. The solid curves show the actual behavior, while dot-dashed and dashed correspond to artificially turning off all $2 \to 2$ or all $3 \to 2$ interactions, respectively, revealing an important interplay between the two. Keeping only the $3 \to 2$ reaction would predict that A' becomes the dominant DM component, whereas in reality it remains highly subdominant. Again the freeze-out process is prolonged, starting with the decoupling of $2 \to 2$ scatterings at $x \sim 20$, while the $3 \to 2$ reactions decouple at $x \sim 150$. Interestingly, $n_{A'}$ temporarily grows between these two times, allowing the $2 \to 2$ rate to come back above H just before freezeout completes.

In fig. 3(b), we plot contours corresponding to the observed thermal relic density in the m_χ-r plane, for different values of α'. In the following we give a brief analytic explanation of the contour shapes in the regions $r < 1$, $1 < r \lesssim 1.5$ and $1.5 < r \lesssim 2$, whose qualitative behavior is distinct.

(1) $r < 1$. Being lighter than χ, A' is the dominant DM constituent. The relic abundance can be qualitatively understood as $Y_{A'} \sim (r x_f)^{3/2} e^{-r x_f}$ where x_f denotes the freezeout of the dominant $3 \to 2$ reactions $\chi\bar{\chi}A' \to \chi\bar{\chi}$ and $\chi\chi A' \to \chi\chi$, whose rates at freezeout scale as $\Gamma \sim \alpha^3 (m_\chi/x_f^3) e^{-2x_f}$. Equating $\Gamma \sim H \sim T^2/m_{\rm pl}$ to estimate x_f gives contours consistent with those shown.

(2) $1 < r \lesssim 1.5$. χ is the dominant DM component. The fastest reaction is $A'A' \leftrightarrow \chi\bar{\chi}$, and it enforces $n_{A'} = n_{A',0} n_\chi/n_{\chi,0}$ during the freezeout of the second-fastest reaction, $\chi\chi\bar{\chi} \to \chi A'$, which determines the DM abundance. The $3 \to 2$ rate goes as $n_\chi^2 \langle\sigma v^2\rangle$, which depends only weakly on r through the phase space. Therefore there is no strong correlation between the abundance and r in this region.

(3) $1.5 \lesssim r \lesssim 2$. χ is the dominant DM component, but now its abundance is determined by the two freezeout events $A'A' \to \chi\bar{\chi}$ (whose rate becomes comparable to Hubble at later times) followed by $\chi\chi\bar{\chi} \to \chi A'$. At large $r \lesssim 2$, just before freezeout completes, both reactions are faster than H, allowing one to estimate the freezeout times. Taking the $2 \to 2$ and $3 \to 2$ rates $\sim H$, and $n_{A'} \simeq n_{A',0}\, n_\chi/n_{\chi,0}$ enforced by fast $3 \to 2$ scatterings, we can analytically derive contours consistent with the numerical results.

III. CONSTRAINTS

The parameter space of NFDM is constrained by a variety of experimental observations: i) dark photon limits on ϵ as a function of $m_{A'}$ coming from the cooling of SN1987a [34]; ii) similar bounds from beam dump experiments [32, 33]; iii) limits on the thermally-averaged cross section of $\chi\bar{\chi} \to e^+e^-$ deduced from the CMB power spectrum measured by Planck [30, 31, 39–41], and iv) direct detection constraints on the dark matter-nucleon

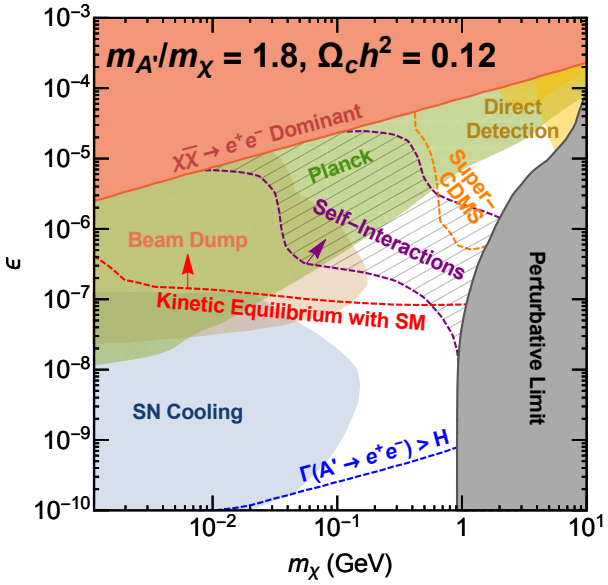

FIG. 4. Constraints in the m_χ-ϵ plane for the case of $m_{A'}/m_\chi = 1.8$, with α' chosen to produce the observed relic density. The upper-left shaded region indicates where freezeout is dominated by the conventional $\chi\bar{\chi} \to e^+e^-$ annihilations. Limits are derived from the CMB power spectrum [30] (green), beam dump experiments [32, 33] (pale orange), SN1987a cooling [34] (blue) and direct detection [35–37] (yellow), perturbativity, $\alpha' \geq 4\pi$ (gray), and the projected reach of SuperCDMS [38] (orange dashed line). Curve near $\epsilon \sim 10^{-7}$ indicates where kinetic equilibrium with SM is established (red dashed line), and cosmological limits $(\sigma/m_\chi)/(\mathrm{cm}^2/\mathrm{g}) < 0.1$ (upper), 1 (lower) on the self-interaction cross section of dark matter (purple dashed lines). The purple arrow points into the region allowed by self-interaction bounds, above and to the right of the line. The A' decay rate is faster than H at freezeout above the lowest (blue) curve.

scattering cross section from PandaX-II [35], LUX [36] and CDMSLite [37]. The projected reach of the SuperCDMS SNOLAB experiment [38] surpasses the current CMB limits on ϵ for $m_\chi \sim 1$ GeV by an order of magnitude, and will be a powerful probe of the available parameter space. Other constraints from indirect detection [42] and lower bounds on m_χ from $N_{\rm eff}$ [43] are weaker than those presented here and are not considered.

Fig. 4 summarizes these constraints in the m_χ-]*epsilon* plane for the illustrative value of $m_{A'}/m_\chi = 1.8$, with α' fixed to give the correct present-day relic density, subject to the perturbativity constraint $\alpha' \leq 4\pi$. At a large ϵ and small m_χ, conventional freezeout from $\chi\bar{\chi} \to e^+e^-$ annihilations dominates over the NFDM mechanism, but this is ruled out by the CMB constraint. The approximately horizontal dashed contour shows the minimum value of ϵ for which the visible and dark sectors are in kinetic equilibrium, estimated in eq. (4).

Self-interactions between dark matter particles with a cross section $\sigma_{\rm SI} \sim 0.1 \lesssim \sigma_{\rm SI}/m_\chi \lesssim 1\ \mathrm{cm}^2\ \mathrm{g}^{-1}$ can potentially resolve the core-cusp and the too-big-to-fail problems of small-structure formation with cold DM [44–46] while remaining consistent with experimental constraints [47]. A DM mass of $m_\chi \sim (0.1 - 1)\,\mathrm{GeV}$ with $\epsilon \sim 10^{-7} - 10^{-6}$ in our model leads to a velocity-independent self-interaction cross section (eq. (15), supplemental material) that lies within this range, and can provide a possible solution to both puzzles (though recent analysis of clusters indicates some preference for a velocity-dependent cross section [48]). The preferred region is between the (purple) dashed lines in fig. 4, while the cosmologically allowed region is above these curves.

IV. SUMMARY AND OUTLOOK

We have demonstrated a novel scenario, "Not-Forbidden Dark Matter", where an allowed $3 \to 2$ annihilation process compensates for its conventional $2 \to 2$ counterpart being kinematically forbidden during thermal freezeout. This mechanism can be potentially important in a variety of hidden sector models, including vector-portal DM, scalar-portal DM, composite DM and possibly others. The DM mass and the mediator (or second DM) mass are of the same order, which would naturally arise in a hidden sector characterized by a single scale.

Taking the dark photon + Dirac DM model as an example, we found that in some parts of the NFDM parameter space, the combined effect of $3 \to 2$, $2 \to 2$ and A' decay channels is to significantly prolong the period of freezeout. The commonly-neglected $3 \to 2$ annihilation channel can change the predicted relic density by orders of magnitude. Although this model is restricted by an abundance of experimental constraints, viable examples remain in the mass range $\sim (0.1 - 10)\,\mathrm{GeV}$, with a self-interaction cross section that is coincidentally of the right order for solving the small scale structure problems of ΛCDM cosmological simulations. This is a well-motivated target for future direct detection [38, 49, 50] and dark photon searches [51–55].

While we were completing this work, [56] appeared, presenting a related idea. Their work focuses on keV-MeV scalar DM and requires additional scalar "assister" particles.

ACKNOWLEDGEMENTS

We thank Lina Necib, Nicholas Rodd and Yotam Soreq for useful discussions. JC is supported by NSERC (Canada) and FRQNT (Québec). HL, TS and WX are supported by the U.S. Department of Energy under grant Contract Numbers DE-SC-00012567 and DE-SC-0013999.

[1] M. Pospelov, A. Ritz, and M. B. Voloshin, Phys. Lett. **B662**, 53 (2008), arXiv:0711.4866 [hep-ph].
[2] N. Arkani-Hamed, D. P. Finkbeiner, T. R. Slatyer, and N. Weiner, Phys. Rev. **D79**, 015014 (2009), arXiv:0810.0713 [hep-ph].
[3] Y. Hochberg, E. Kuflik, T. Volansky, and J. G. Wacker, Phys. Rev. Lett. **113**, 171301 (2014), arXiv:1402.5143 [hep-ph].
[4] Y. Hochberg, E. Kuflik, H. Murayama, T. Volansky, and J. G. Wacker, Phys. Rev. Lett. **115**, 021301 (2015), arXiv:1411.3727 [hep-ph].
[5] H. M. Lee and M.-S. Seo, Phys. Lett. **B748**, 316 (2015), arXiv:1504.00745 [hep-ph].
[6] Y. Hochberg, E. Kuflik, and H. Murayama, JHEP **05**, 090 (2016), arXiv:1512.07917 [hep-ph].
[7] N. Bernal, X. Chu, and J. Pradler, (2017), arXiv:1702.04906 [hep-ph].
[8] R. T. D'Agnolo and A. Hook, Phys. Rev. **D91**, 115020 (2015), arXiv:1504.00361 [hep-ph].
[9] R. T. D'Agnolo and J. T. Ruderman, Phys. Rev. Lett. **115**, 061301 (2015), arXiv:1505.07107 [hep-ph].
[10] A. Delgado, A. Martin, and N. Raj, (2016), arXiv:1608.05345 [hep-ph].
[11] E. D. Carlson, M. E. Machacek, and L. J. Hall, Astrophys. J. **398**, 43 (1992).
[12] D. Pappadopulo, J. T. Ruderman, and G. Trevisan, Phys. Rev. **D94**, 035005 (2016), arXiv:1602.04219 [hep-ph].
[13] N. Bernal, X. Chu, C. Garcia-Cely, T. Hambye, and B. Zaldivar, JCAP **1603**, 018 (2016), arXiv:1510.08063 [hep-ph].
[14] E. Kuflik, M. Perelstein, N. R.-L. Lorier, and Y.-D. Tsai, Phys. Rev. Lett. **116**, 221302 (2016), arXiv:1512.04545 [hep-ph].
[15] N. Bernal and X. Chu, JCAP **1601**, 006 (2016), arXiv:1510.08527 [hep-ph].
[16] M. Farina, D. Pappadopulo, J. T. Ruderman, and G. Trevisan, (2016), arXiv:1607.03108 [hep-ph].
[17] J. A. Dror, E. Kuflik, and W. H. Ng, (2016), arXiv:1607.03110 [hep-ph].
[18] S. Okawa, M. Tanabashi, and M. Yamanaka, (2016), arXiv:1607.08520 [hep-ph].
[19] P. Bandyopadhyay, E. J. Chun, and J.-C. Park, JHEP **06**, 129 (2011), arXiv:1105.1652 [hep-ph].
[20] F. D'Eramo and J. Thaler, JHEP **06**, 109 (2010), arXiv:1003.5912 [hep-ph].
[21] K. Agashe, Y. Cui, L. Necib, and J. Thaler, JCAP **1410**, 062 (2014), arXiv:1405.7370 [hep-ph].
[22] J. Berger, Y. Cui, and Y. Zhao, JCAP **1502**, 005 (2015), arXiv:1410.2246 [hep-ph].
[23] J. Kopp, J. Liu, and X.-P. Wang, JHEP **04**, 105 (2015), arXiv:1503.02669 [hep-ph].
[24] A. Berlin, D. Hooper, and G. Krnjaic, Phys. Lett. **B760**, 106 (2016), arXiv:1602.08490 [hep-ph].
[25] J. Kopp, J. Liu, T. R. Slatyer, X.-P. Wang, and W. Xue, JHEP **12**, 033 (2016), arXiv:1609.02147 [hep-ph].
[26] F. Kahlhoefer, K. Schmidt-Hoberg, T. Schwetz, and S. Vogl, JHEP **02**, 016 (2016), arXiv:1510.02110 [hep-ph].
[27] J. A. Adams, S. Sarkar, and D. Sciama, Mon.Not.Roy.Astron.Soc. **301**, 210 (1998), arXiv:astro-ph/9805108 [astro-ph].
[28] X.-L. Chen and M. Kamionkowski, Phys. Rev. **D70**, 043502 (2004), astro-ph/0310473.
[29] N. Padmanabhan and D. P. Finkbeiner, Phys. Rev. **D72**, 023508 (2005), astro-ph/0503486.
[30] P. A. R. Ade et al. (Planck), Astron. Astrophys. **594**, A13 (2016), arXiv:1502.01589 [astro-ph.CO].
[31] T. R. Slatyer, Phys. Rev. **D93**, 023527 (2016), arXiv:1506.03811 [hep-ph].
[32] J. D. Bjorken, R. Essig, P. Schuster, and N. Toro, Phys. Rev. **D80**, 075018 (2009), arXiv:0906.0580 [hep-ph].
[33] S. Andreas, C. Niebuhr, and A. Ringwald, Phys. Rev. **D86**, 095019 (2012), arXiv:1209.6083 [hep-ph].
[34] J. B. Dent, F. Ferrer, and L. M. Krauss, (2012), arXiv:1201.2683 [astro-ph.CO].
[35] A. Tan et al. (PandaX-II), Phys. Rev. Lett. **117**, 121303 (2016), arXiv:1607.07400 [hep-ex].
[36] D. S. Akerib et al. (LUX), Phys. Rev. Lett. **116**, 161301 (2016), arXiv:1512.03506 [astro-ph.CO].
[37] R. Agnese et al. (SuperCDMS), Phys. Rev. Lett. **116**, 071301 (2016), arXiv:1509.02448 [astro-ph.CO].
[38] R. Agnese et al. (SuperCDMS), Submitted to: Phys. Rev. D (2016), arXiv:1610.00006 [physics.ins-det].
[39] D. P. Finkbeiner, S. Galli, T. Lin, and T. R. Slatyer, Phys. Rev. **D85**, 043522 (2012), arXiv:1109.6322 [astro-ph.CO].
[40] T. R. Slatyer, N. Padmanabhan, and D. P. Finkbeiner, Phys. Rev. **D80**, 043526 (2009), arXiv:0906.1197 [astro-ph.CO].
[41] H. Liu, T. R. Slatyer, and J. Zavala, Phys. Rev. **D94**, 063507 (2016), arXiv:1604.02457 [astro-ph.CO].
[42] R. Essig, E. Kuflik, S. D. McDermott, T. Volansky, and K. M. Zurek, JHEP **11**, 193 (2013), arXiv:1309.4091 [hep-ph].
[43] C. Boehm, M. J. Dolan, and C. McCabe, JCAP **1308**, 041 (2013), arXiv:1303.6270 [hep-ph].
[44] M. Rocha, A. H. G. Peter, J. S. Bullock, M. Kaplinghat, S. Garrison-Kimmel, J. Onorbe, and L. A. Moustakas, Mon. Not. Roy. Astron. Soc. **430**, 81 (2013), arXiv:1208.3025 [astro-ph.CO].
[45] D. N. Spergel and P. J. Steinhardt, Phys. Rev. Lett. **84**, 3760 (2000), arXiv:astro-ph/9909386 [astro-ph].
[46] J. Zavala, M. Vogelsberger, and M. G. Walker, Monthly Notices of the Royal Astronomical Society: Letters **431**, L20 (2013), arXiv:1211.6426 [astro-ph.CO].
[47] D. Harvey, R. Massey, T. Kitching, A. Taylor, and E. Tittley, Science **347**, 1462 (2015), arXiv:1503.07675 [astro-ph.CO].
[48] M. Kaplinghat, S. Tulin, and H.-B. Yu, Phys. Rev. Lett. **116**, 041302 (2016), arXiv:1508.03339 [astro-ph.CO].
[49] R. Essig, J. Mardon, and T. Volansky, Phys. Rev. **D85**, 076007 (2012), arXiv:1108.5383 [hep-ph].
[50] S. Derenzo, R. Essig, A. Massari, A. Soto, and T.-T. Yu, (2016), arXiv:1607.01009 [hep-ph].
[51] P. Ilten, J. Thaler, M. Williams, and W. Xue, Phys. Rev. **D92**, 115017 (2015), arXiv:1509.06765 [hep-ph].
[52] P. Ilten, Y. Soreq, J. Thaler, M. Williams, and W. Xue, Phys. Rev. Lett. **116**, 251803 (2016), arXiv:1603.08926 [hep-ph].
[53] S. Alekhin et al., Rept. Prog. Phys. **79**, 124201 (2016), arXiv:1504.04855 [hep-ph].

[54] S. Gardner, R. J. Holt, and A. S. Tadepalli, Phys. Rev. **D93**, 115015 (2016), arXiv:1509.00050 [hep-ph].
[55] O. Moreno (2013) arXiv:1310.2060 [physics.ins-det].
[56] U. K. Dey, T. N. Maity, and T. S. Ray, (2016), arXiv:1612.09074 [hep-ph].

SUPPLEMENTAL MATERIAL

Here we provide further details concerning the distinctive features of the NFDM freezeout mechanism, and how it differs from the usual $2 \to 2$ annihilation scenario.

A. Coupled Boltzmann equations and prolonged freezeout

As mentioned above, an essential difference between NFDM and conventional DM freezeout is the importance of tracking the evolution of both the DM χ and the mediator particle (in our model, A'), by solving the coupled Boltzmann equations (2, 3) for their respective densities. The presence of two equations implies that more than one scattering (or decay) process can be important for determining the final abundance; hence both the fastest and second fastest reactions are typically relevant.

This is in contrast to conventional DM freezeout based upon a single Boltzmann equation, where the abundance depends upon the strongest channel. In the large ϵ limit of our model, A' decay is the fastest process, and enforces equilibrium of A', $n_A = n_{A',0}$. Hence smaller values of ϵ are necessary to realize the rich cosmology that comes from the interplay of the coupled Boltzmann equations of χ and A'. To simplify the subsequent discussion, we assume that these ϵ-suppressed reactions are negligibly slow, i.e. we work in the secluded dark sector regime of the NFDM model.

It is useful to define the net rate of $3 \leftrightarrow 2$ or $2 \leftrightarrow 2$ interactions per χ or A' particle by considering the collision terms in the Boltzmann equations, written in the form $R_\chi \equiv d\log n_\chi/dt = -3Hn_\chi - R_\chi(3 \leftrightarrow 2) + R_\chi(2 \leftrightarrow 2)$ and $R_{A'} \equiv d\log n_{A'}/dt = -3Hn_{A'} + R_{A'}(3 \leftrightarrow 2) - R_{A'}(2 \leftrightarrow 2)$, where

$$\begin{aligned} R_\chi(3 \leftrightarrow 2) &\equiv 2\frac{n_{A'}}{n_\chi} R_{A'}(3 \leftrightarrow 2) \qquad (5)\\ &= \frac{1}{4}\langle\sigma v^2\rangle_{\chi\chi\bar\chi\to\chi A'}\left(n_\chi^2 - n_{\chi,0}^2\frac{n_{A'}}{n_{A',0}}\right)\\ &\equiv R_\chi(\chi\chi\bar\chi \to \chi A') - R_\chi(\chi A' \to \chi\chi\bar\chi), \end{aligned}$$

$$\begin{aligned} R_\chi(2 \leftrightarrow 2) &\equiv \frac{n_{A'}}{n_\chi} R_{A'}(2 \leftrightarrow 2) \qquad (6)\\ &= \langle\sigma v\rangle_{A'A'\to\bar\chi\chi}\left(\frac{n_{A'}^2}{n_\chi} - \frac{n_{A',0}^2 n_\chi}{n_{\chi,0}^2}\right)\\ &\equiv R_\chi(A'A' \to \bar\chi\chi) - R_\chi(\bar\chi\chi \to A'A'). \end{aligned}$$

Likewise, we define $2(n_{A'}/n_\chi)R_{A'}(\chi\chi\bar\chi \to \chi A') \equiv R_\chi(\chi\chi\bar\chi \to \chi A')$ and so on for the unidirectional rates. In this way, the signs for these definitions have been chosen so that all of the rates of individual sub-processes are now positive, although the overall rates R_χ and $R_{A'}$ can have any sign. When $m_{A'} > m_\chi$ and $T < m_\chi, m_{A'}$, the lower density of A' relative to χ implies that $R_\chi(3 \leftrightarrow 2)$ ($R_\chi(2 \leftrightarrow 2)$) is generally smaller in magnitude than $R_{A'}(3 \leftrightarrow 2)$ ($R_{A'}(2 \leftrightarrow 2)$). Thus the rates R_χ tend to fall below H earlier than the corresponding rates $R_{A'}$. This separation between freezeout of χ and A' is the origin of the prolonged duration of the overall freezeout process.

Suppose that only one channel, for example $2 \to 2$, occurs fast enough such that $R_\chi(A'A' \to \bar\chi\chi) \gg H$; then this rate tends to be nearly equal to that of the reverse reaction, $R_\chi(\bar\chi\chi \to A'A')$, enforcing the condition $n_{A'}^2 \simeq n_{A',0}^2\, n_\chi^2/n_{\chi,0}^2$ (though the cancellation is imperfect, so that the total rate $R_\chi(2 \leftrightarrow 2)$ is also typically greater than H). This by itself is not sufficient to force both the χ and A' densities to track their equilibrium values. For that, one generically needs both $R_\chi(3 \leftrightarrow 2) > H$ and $R_\chi(2 \leftrightarrow 2) > H$ so that both independent combinations $n_\chi - n_{\chi,0}$ and $n_{A'} - n_{A',0}$ are driven to zero [1]. This is always true at sufficiently early times, allowing us to use equilibrium initial conditions for the Boltzmann equations. The DM density n_χ starts to deviate from equilibrium when the rate of the weaker annihilation channel becomes comparable to H; hence the second-strongest channel initiates the freezeout process.

To illustrate this behavior, we show some examples of the evolution of the rates in fig. 5a, 5b and 6. Each example has the same DM mass $m_\chi = 70$ MeV, coupling $\alpha' = 1$, and kinetic mixing $\epsilon = 0$, but different values of $r = 1.4,\ 1.7,\ 1.9$. In these figures, the dot-dashed lines corresponding to the evolution of DM number density are shown to highlight the time of DM freezeout. For $r = 1.4$, the freezeout period is relatively short; for $r = 1.7$, freezeout is prolonged; and for $r = 1.9$, the freezeout is prolonged further and may indeed be thought of as two separated freezeouts.

In fig. 5b, we show the two rates $R_{A'}(3 \leftrightarrow 2)$ and $R_{A'}(2 \leftrightarrow 2)$, which are much larger than H; these cancel each other to order H. The behavior is similar for other values of r. Since $R_{A'}(3 \leftrightarrow 2) \simeq R_A(2 \leftrightarrow 2)$, eq. (5,6) implies that $R_\chi(3 \leftrightarrow 2) \simeq 2R_\chi(2 \leftrightarrow 2)$. This relation is demonstrated in fig. 5a,6.

Comparing these net rates however does not tell us which process controls the freezeout. Instead, we should look at the dashed lines, which indicate the unidirectional rates, $R_\chi(A'A' \to \bar\chi\chi)$ and $R_\chi(\chi\chi\bar\chi \to \chi A')$. Processes are out of equilibrium when these dashed lines overlap with the solid lines. From the unidirectional rates, we can identify the weaker annihilation channel and thus which process initiates the freezeout. For $r = 1.4$, the weaker process is $3 \to 2$, and fig. 5a confirms that the freezeout is indeed triggered by $3 \to 2$. For $r = 1.7$ and $r = 1.9$, the dashed line for $R_\chi(A'A' \to \bar\chi\chi)$ in fig. 6 merges with the solid line, $R_\chi(2 \leftrightarrow 2)$, when the rate is about $3H$. It is the weaker channel $2 \to 2$ that initiates freezeout.

---

[1] The typical behavior is that the strongest process is such that both the forward and backward rates exceed H, as well as their difference. For the second-strongest, only one of these need be greater than H.

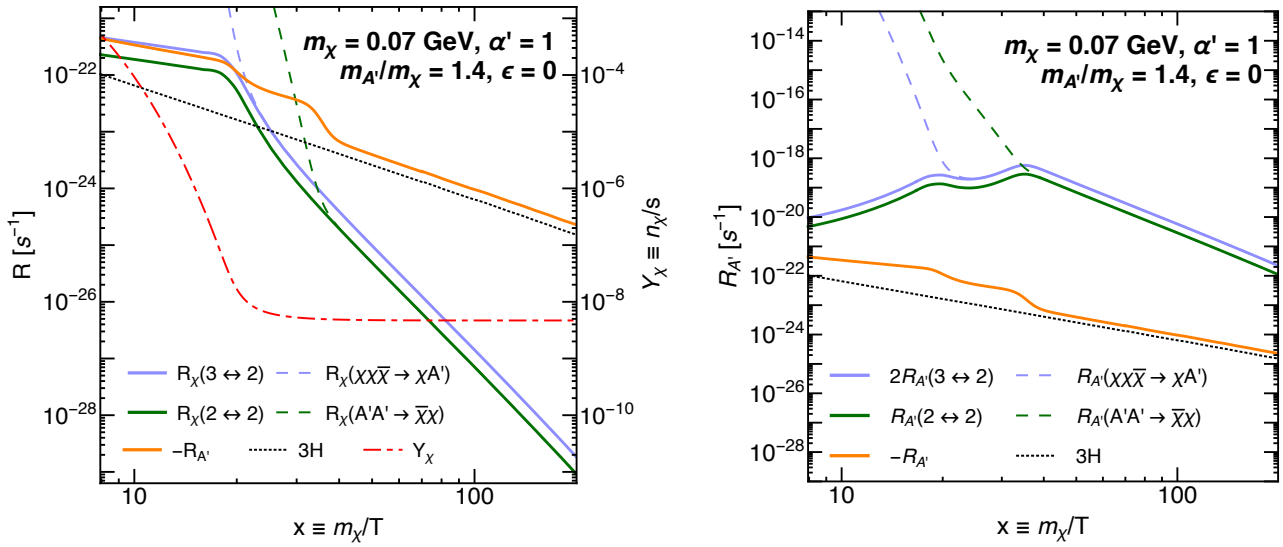

(a) (b)

FIG. 5. Rates of different processes during freezeout for $m_{A'}/m_\chi = 1.4$: (a) evolution of $R_\chi(3 \leftrightarrow 2)$ (light blue), $R_\chi(2 \leftrightarrow 2)$ (green) and the A' total rate $R_{A'}$ (orange) as a function of $x \equiv m_\chi/T$. Rates for processes in one direction, $R_\chi(\chi\chi\bar{\chi} \to A'\chi)$ (light blue, dashed) and $R_\chi(A'A' \to \chi\bar{\chi})$ (green, dashed) are also shown. The dark matter abundance Y_χ (red, dot-dashed) is plotted, with the appropriate (dimensionless) units given on the right-hand axis; (b) evolution of $R_{A'}(3 \leftrightarrow 2)$ (light blue), $R_{A'}(2 \leftrightarrow 2)$ (green) and the A' total rate $R_{A'}$ (orange) as a function of x. Rates for processes in one direction, $R_{A'}(\chi\chi\bar{\chi} \to A'\chi)$ (light blue, dashed) and $R_{A'}(A'A' \to \chi\bar{\chi})$ (green, dashed) are also shown. The evolution of the Hubble rate H (black, dotted) is shown in both plots for reference.

One difference between $r < 1.5$ and $r > 1.5$ in figs. 5a versus 6 is that $r > 1.5$ normally has a longer freezeout. The duration depends upon whether the rate of the weaker annihilation channel is sensitive to $n_{A'}$. For $r > 1.5$, the weaker process $2 \to 2$ has the rate $R \sim \langle\sigma v\rangle_{A'A' \to \bar{\chi}\chi} n_{A'}^2/n_\chi$. Prior to the final freezeout, the larger $3 \to 2$ rate imposes the constraint that $n_{A'} \simeq n_{A',0} n_\chi^2/n_{\chi,0}^2 \sim r^{3/2}x^{3/2}m^{-3}\exp((2-r)x)n_\chi^2$. Since $n_{A'}$ increases with time, this means that the $2 \to 2$ rate $R_\chi(A'A' \to \bar{\chi}\chi)$ can be kept at the same order as H for a long period. For this reason, the freezeout is prolonged. For $r < 1.5$, the duration is relatively short, because the rate of the weaker $3 \to 2$ process goes as $R_\chi(\chi\chi\bar{\chi} \to \chi A') \propto n_\chi^2$, where n_χ is decreasing with time.

Armed with our insight that the second-strongest channel matters critically for freezeout, and having understood the reason that the freezeout process is longer for $r \gtrsim 1.5$, we can also explain the shape of the contours in fig. 2(b). As discussed briefly in the main text, there are several important regimes:

1. For $n_{A'} = n_{A',0}$, corresponding to large ϵ, the two Boltzmann equations are reduced to one, and the shape of the contours can be understood using the usual parametrics of DM freezeout. This behavior occurs for the contours overlapping the dashed contours in fig. 2(b).

2. For $\epsilon = 0$, we recover the secluded case discussed above, where the interplay of the $3 \leftrightarrow 2$ and $2 \leftrightarrow 2$ processes controls the freezeout. This behavior also occurs in the region where $r \sim 1.5$ and $\alpha' = 10$, because the $3 \to 2$ and $2 \to 2$ rates for DM are significantly larger than $R_\chi(A' \to e^+e^-)$, so that $\Gamma_{A' \to e^+e^-}$ can be neglected.

3. For moderate ϵ, the rates of the three processes should be compared in order to determine which is weakest, and hence irrelevant to the DM freezeout. The relevant rates to compare are $R_\chi(\chi\bar{\chi}\chi \to A'\chi)$, $R_\chi(A'A' \to \chi\bar{\chi})$ and $R_\chi(A' \to e^+e^-) \equiv \Gamma(A' \to e^+e^-)n_{A'}/n_\chi$, evaluated at the Hubble crossing time of the annihilation processes.[2] Consider the case where $2 \to 2$ has a lower rate than $3 \to 2$, such that it falls below H first. Whether the DM density freezes out or not at this time depends on the relative sizes of $R_\chi(A' \to e^+e^-)$ and $R_\chi(A'A' \to \chi\bar{\chi})$. When $R_\chi(A'A' \to \chi\bar{\chi}) < R_\chi(A' \to e^+e^-)$, the larger $R_\chi(A' \to e^+e^-)$ rate in the coupled Boltzmann equations provides enough constraints to keep n_χ and $n_{A'}$ near their equilibrium values. An example of this more complex case is shown in fig. 2(a), where

[2] We define the A' decay rate with respect to the DM density, $R_\chi(A' \to e^+e^-)$; even though this quantity does not appear in Boltzmann equation of DM, the coupling to the A' Boltzmann equation will cause $A' \to e^+e^-$ to play an important role in determining the rate for DM processes in some cases.

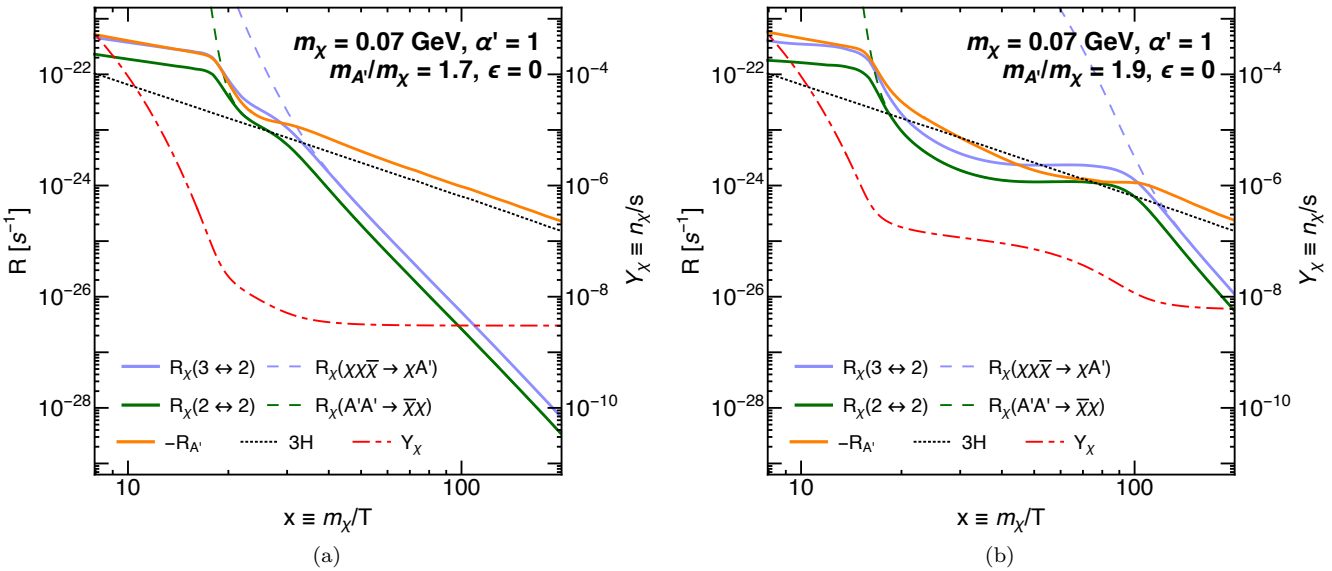

FIG. 6. Same as fig. 5a, but with (a) $m_{A'}/m_\chi = 1.7$, and (b) $m_{A'}/m_\chi = 1.9$.

the freezeout starts when $R_\chi(3 \leftrightarrow 2) \sim H$. Using the Boltzmann equation of A', this rate is determined by the A' decay, $R_\chi(3 \leftrightarrow 2) \sim 2R_\chi(A' \to e^+e^-)$; freeze-out then terminates when $R_\chi(\chi\bar{\chi}\chi \to A'\chi) \sim H$.

More broadly, this case is realized when $\epsilon = 10^{-6}$, and either r is close to 2, or α' is large and $r > 1.5$. From fig. 2(b), we see that in this region the $\epsilon = 10^{-6}$ contours (solid lines) do not overlap with the dashed contours, for which the constraint $n_{A'} = n_{A',0}$ is imposed. In this regime the $3 \to 2$ rate is the largest, and when $R_\chi(A'A' \to \chi\bar{\chi}) \sim H$, $R_\chi(A' \to e^+e^-) > R_\chi(A'A' \to \chi\bar{\chi})$. The freezeout is thus controlled by $3 \to 2$ processes and the decay of A'. In this case the A' decay rate is not fast enough to keep the A' abundance in equilibrium, and both $n_{A'}$ and n_χ are increased during freezeout relative to their values when the A's remain in equilibrium. The χ annihilation rate thus needs to be increased to maintain the correct relic density, requiring lower χ masses; this is the reason that the contours in fig. 2(b) bend toward lower masses as ϵ is decreased, for large r.

B. Dependence on T_d

If the dark sector is secluded, its temperature T_d may differ from that of the visible sector, $T_{\rm SM}$. This difference affects the evolution of the χ and A' densities and ultimately the DM relic abundance. In the Boltzmann equations (2, 3), taking $T_d \neq T_{\rm SM}$ changes the equilibrium densities, so that $n_{\chi,0} \sim \exp(-m_\chi/T_d) = \exp(-x/\gamma)$, where we have defined $\gamma \equiv T_d/T_{\rm SM}$, and x is still given by $x \equiv m_\chi/T_{\rm SM}$. Likewise, $n_{A',0} \sim \exp(-rx/\gamma)$. Keeping in mind that H is determined by $T_{\rm SM}$, we can solve the Boltzmann equations for $n_\chi(x)$ and $n_{A'}(x)$ with the γ-dependence coming from the equilibrium densities.

Fig. 7 shows the behavior of the ratio of relic abundances $\Omega_c(T_d)/\Omega_c(T_d = T_{\rm SM})$ as a function of T_d for $0.1 \leq \gamma \leq 1$. Having $T_d < T_{\rm SM}$ leads to an earlier freezeout, since the exponential decrease in the equilibrium densities occurs more rapidly. For values of r where the backward and forward $3 \to 2$ processes fall out of equilibrium at freezeout, we expect that $n_\chi^2 \sim H/\langle\sigma v^2\rangle_{\chi\chi\bar{\chi}\to\chi A'} \sim 1/x_f^2$, and therefore that the relic abundance scales as $\Omega_c \sim x_f^2$. For $1 < r \lesssim 1.5$ where the $3 \to 2$ process determines the DM abundance, the exponential dependence of $n_{\chi,0}$ with x/γ results in $\Omega_c \sim \gamma^2$. On the other hand, in the case of $r \lesssim 2$, the second freezeout occurs at $n_\chi \propto n_{\chi,0}^4/n_{A',0}^2$, and a similar argument leads again to $\Omega_c \sim \gamma^2$. At intermediate values of r, both the $3 \to 2$ and $2 \to 2$ processes freeze out at similar times. For a $2 \to 2$ freezeout, $n_\chi \sim H/\langle\sigma v\rangle_{\bar{\chi}\chi\to A'A'}$, and as a result $\Omega_c \sim \gamma$. Qualitatively, we expect the γ dependence to lie between these two regimes for intermediate values of r.

C. Constraints at different r

Fig. 8 shows the constraints in the ϵ-m_χ plane for two representative values of r, with α' fixed to give the correct present-day relic density. These have the same general features as in fig. 4, but also exhibit several distinct characteristics that we explain here.

At $r = 1.4$, the transition from the secluded limit ($\epsilon \to 0$) to the kinetic equilibrium limit occurs in the range $\epsilon \sim 10^{-9} - 10^{-6}$, which leads to a rapid decrease in α' between these two phases at a fixed value of m_χ. This explains the rapid change in the behavior of the region

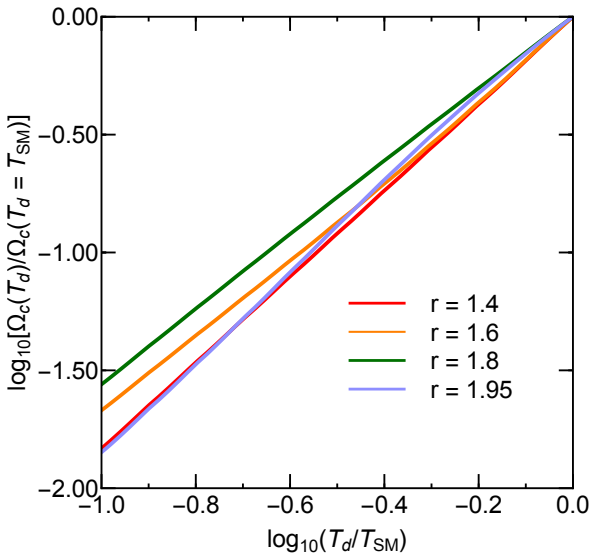

FIG. 7. Ratio of the relic abundance when $T_d < T_{\rm SM}$ to the relic abundance with $T_d = T_{\rm SM}$ as a function of $\gamma \equiv T_d/T_{\rm SM}$ for $r \equiv m_{A'}/m_\chi = 1.4$ (red), 1.6 (orange), 1.8 (green) and 1.95 (light blue).

with suitable self-interaction for $m_\chi \lesssim 100$ MeV.

At $r = 1.6$, the most distinctive feature is the change in behavior of the region where annihilations to e^+e^- dominates at $m_\chi \sim 100$ MeV. At masses smaller than this point, the $2 \to 2$ process is freezes out last, while at larger masses, it is the $3 \to 2$ process which does so. This difference accounts for the change in the slope of the boundary. There is no such transition for the other two cases, since at $r = 1.8$, the $3 \to 2$ process always freezes out last, while for $r = 1.4$ it is the $2 \to 2$ process instead.

For all values of r, a significant part of the ϵ-m_χ parameter space is still consistent with the present-day relic density while evading experimental constraints, showing that the NFDM scenario is robust against taking different values of $r \gtrsim 1.5$.

D. Cross sections and decay rates

The decay rate for $A' \to e^+e^-$ is

$$\Gamma(A' \to e^+e^-) = \frac{\epsilon^2 \alpha_{em}}{3} m_{A'} \left(1 + 2\frac{m_e^2}{m_{A'}^2}\right) \sqrt{1 - 4\frac{m_e^2}{m_{A'}^2}} \,. \tag{7}$$

For simplicity we give the following cross sections at the kinematic threshold, with the exception of $\chi e^\pm \to \chi e^\pm$. We define $r \equiv m_{A'}/m_\chi$.

- $\chi\bar{\chi} \to A'A'$: for the case where $r < 1$,

$$\langle \sigma v \rangle = \frac{g'^4 \left(1 - r^2\right)^{3/2}}{4\pi\, m_\chi^2 \left(r^2 - 2\right)^2} \,. \tag{8}$$

- $A'A' \to \chi\bar{\chi}$: for the case where $r > 1$,

$$\langle \sigma v \rangle = \frac{4 g'^4 \sqrt{r^2 - 1}\left(r^4 + r^2 - 2\right)}{9\pi\, m_\chi^2\, r^7} \,. \tag{9}$$

- $\chi e^\pm \to \chi e^\pm$: to determine kinetic equilibrium of the DM, we are interested in this process, including the full thermal average.

$$\langle \sigma v \rangle = \frac{2(g'\epsilon e)^2 \mu_{e\chi}^2}{\pi m_{A'}^4} \left(\frac{2T}{\pi \mu_{e\chi}}\right)^{1/2} \,, \tag{10}$$

where $\mu_{e\chi}$ is the electron-DM reduced mass, and we have assumed $T < \mu_{e\chi}$. At high temperature, it approaches the limit

$$\langle \sigma v \rangle \to \frac{(g'\epsilon e)^2}{4\pi m_{A'}^2} \,. \tag{11}$$

To get accurate results however, we must use the exact thermal average over the cross section for $\chi e^\pm \to \chi e^\pm$, given by:

$$\sigma = \frac{(g'\epsilon e)^2}{8\pi} \left[\frac{1}{s} + \frac{2}{r^2 m_\chi^2} + \frac{8m_e^2 + r^4 m_\chi^2}{r^2[h(m_\chi, s) + r^2 m_\chi^2 s]} - \frac{2(r^2 m_\chi^2 + s)}{h(m_\chi, s)} \log\left(1 + \frac{h(m_\chi, s)}{r^2 m_\chi^2 s}\right)\right] \,, \tag{12}$$

where $h(m_\chi, s) = (m_\chi^2 - s)^2 - 2m_e^2(m_\chi^2 + s) + m_e^4$. and the thermal average is given by

$$\langle \sigma v \rangle = \frac{1}{8T m_\chi^2 m_e^2 K_2(m_\chi/T) K_2(m_e/T)} \cdot \int_{(m_\chi + m_e)^2}^\infty \frac{ds}{\sqrt{s}} \left((s - m_\chi^2 - m_e^2)^2 - 4m_\chi^2 m_e^2\right) \sigma \,. \tag{13}$$

- $\chi\chi\bar{\chi} \to \chi A'$: for this process we need $r < 2$:

$$\langle \sigma v^2 \rangle = g'^6 \sqrt{r^4 - 20r^2 + 64}\, \left(28672 - 8768\, r^2 + 11476\, r^4 - 1186\, r^6 + 191\, r^8 - 10\, r^{10}\right) / \left[3456\, \pi\, m_\chi^5 (r^2 + 2)^2 \left(r^2 - 4\right)^4\right] \,. \tag{14}$$

- $\chi\chi A' \to \chi\chi$:

$$\langle \sigma v^2 \rangle = \frac{g'^6 \sqrt{r(r+1)}\,(r+4)}{8\pi\, m_\chi^5\, r^4 (r+1)^2 (r+2)^3} \,. \tag{15}$$

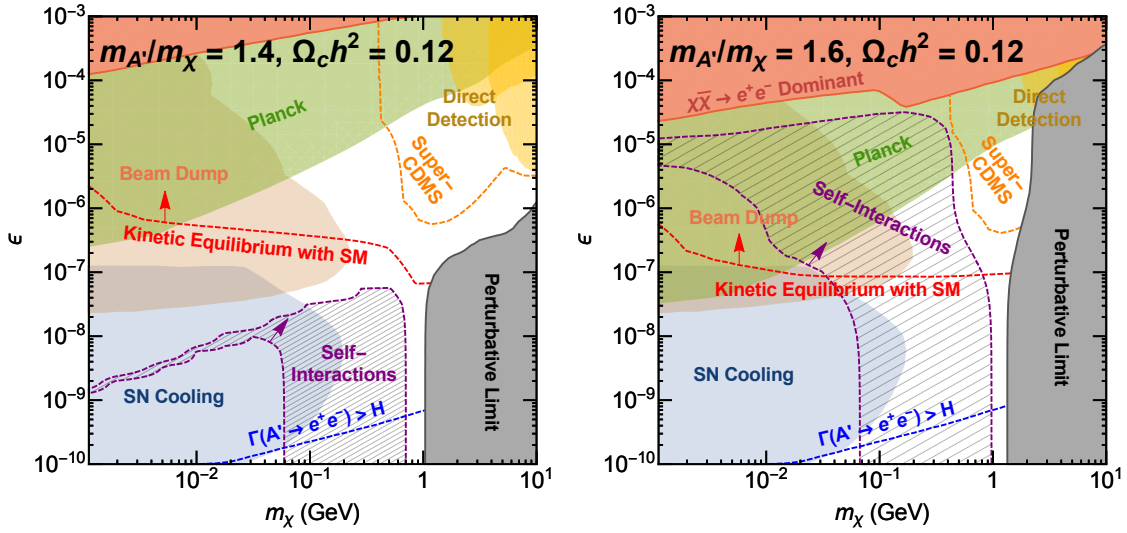

(a) (b)

FIG. 8. Same as fig. 4, but with (a) $m_{A'}/m_\chi = 1.4$, and (b) $m_{A'}/m_\chi = 1.6$.

- $\chi\bar{\chi}A' \to \chi\bar{\chi}$:

$$\langle\sigma v^2\rangle = \frac{g'^6\sqrt{r(r+1)}\left(r^7 - 4r^6 - 17r^5 + 98r^4 + 118r^3 - 272r^2 - 128r + 1664\right)}{48\pi\, m_\chi^5\,(r-2)^2 r^4 (r+1)^2 (r+2)^3}\,. \tag{16}$$

- $\chi\chi \to \chi\chi$: the self-interaction cross section, averaged over particle-particle and particle-antiparticle scattering, is [9]:

$$\frac{\sigma_{\rm SI}}{m_\chi} = \frac{3g'^4}{16\pi m_\chi^3}\frac{16 - 16r^2 + 5r^4}{r^4(r^2-4)^2}\,. \tag{17}$$

- $\chi\bar{\chi} \to e^+e^-$: for the conventional annihilation channel $\chi\bar{\chi} \to e^+e^-$ we find

$$\langle\sigma v\rangle = \frac{\epsilon^2 e^2 g'^2\,(1+\eta^2/2)(1-\eta^2)^{1/2}}{8\pi\, m_\chi^2\,(1-r^2/4)^2}\,, \tag{18}$$

where $\eta \equiv m_e/m_\chi$.